

# Physics of High-Mass Dimuon Production at the 50-GeV Proton Synchrotron

J. C. Peng, G. T. Garvey, J. M. Moss

*Physics Division, LANL, Los Alamos, NM 87545, USA*

S. Sawada, J. Chiba

*KEK, 1-1 Oho, Tsukuba, Ibaraki 305-0801, Japan*

July 28, 2000

## Abstract

We discuss the physics interest and the experimental feasibility for detecting high-mass dimuon pairs using the planned 50-GeV Proton Synchrotron (PS) at the KEK/JHF and JAERI/NSP joint accelerator project. The Drell-Yan measurement of  $p + d$  versus  $p + p$  at 50 GeV will provide unique information on the flavor asymmetry of proton's up and down sea-quark distributions in the large- $x$  region. A study of the nuclear dependences of Drell-Yan cross sections can reveal the modification of antiquark distributions in nuclei. Furthermore, the effect of energy loss for fast partons traversing nuclear medium could also be sensitively measured. If polarized proton beam becomes available at the 50-GeV PS, unique information on the sea-quark polarization could be obtained. Study of heavy quarkonium production at the 50-GeV PS can set important constraints on the mechanism of vector meson productions. Using a prototype dimuon spectrometer, we have simulated the sensitivities for a variety of measurements.

# 1 Introduction

One of the most active areas of research in nuclear and particle physics during the last several decades is the study of quark and gluon distributions in the nucleons and nuclei. Several major surprises were discovered in Deep-Inelastic Scattering (DIS) experiments which profoundly changed our views of the partonic substructure of hadrons. In the early 1980's, the famous 'EMC' effect found in muon DIS provided the first unambiguous evidence that the quark distributions in nuclei are significantly different from those in free nucleons [1, 2]. More recently, surprising results on the spin and flavor structures of the nucleons were discovered in DIS experiments. The so-called 'spin crisis', revealed by the disagreement between the prediction of the Ellis-Jaffe sum rule and the polarized DIS experiments, has led to extensive theoretical and experimental efforts to understand the partonic content of proton's spin [3]. Subsequently, the observation [4] of the violation of the Gottfried sum rule [5] in DIS revealed a surprisingly large asymmetry between the up and down antiquark distributions in the nucleon, shedding new light on the origins of the nucleon sea.

The partonic structure of nucleons and nuclei can also be measured with hadronic probes. A powerful tool for such studies is the Drell-Yan process [6], in which a quark annihilates with an antiquark forming a virtual photon which subsequently decays into a lepton pair. The proton-induced Drell-Yan process is of particular interest, since it can be used to extract antiquark distributions of the target nucleon and nuclei. This provides information complementary to what can be obtained in DIS, which is sensitive to the sum of the quark and antiquark distributions.

The usefulness of the Drell-Yan process as a tool for probing antiquark distributions has been well demonstrated by a series of Fermilab dimuon production experiments [7]. In particular, the Drell-Yan cross section ratios for  $p+d$  versus  $p+p$  led to a direct measurement of the  $\bar{d}/\bar{u}$  asymmetry as a function of Bjorken- $x$  [8, 9]. Furthermore, the nuclear dependence of the Drell-Yan cross sections showed no evidence for antiquark enhancement in heavy nuclei [10], in striking disagreements with predictions of some theoretical models which were capable of explaining the EMC effect.

The 50-GeV Proton Synchrotron (PS) offers a unique opportunity to extend existing measurements of antiquark distributions to much larger values of Bjorken- $x$ . Such information is crucial for understanding the origins of flavor asymmetry in the nucleon sea, and for illuminating the nuclear environment effects on parton distributions. Moreover, Drell-Yan measurements using polarized proton beam on polarized target at the 50-GeV PS will provide a first determination of the spin-dependent antiquark distribution at an  $x$  region not accessible in the RHIC-spin program. Indeed, the flavor asymmetry of polarized sea quark distributions, predicted to be very large by certain theoretical models [11, 12], can be directly measured.

A detailed study of the nuclear dependence of Drell-Yan cross sections at 50 GeV could also lead to a first observation of the coherent partonic energy-loss effects predicted recently by Baier, Dokshitser, Mueller, Peigne, Schiff (BDMPS) [13] and by Zakharov [14]. These authors studied the radiative energy loss (through gluon emission) of high energy partons passing through hot and cold hadronic matter. The partonic energy-loss effect is the QCD analog of the Landau-Pomeranchuk-Migdal (LPM) QED effect [15, 16] predicted over 40 years ago and confirmed only recently at SLAC [17]. A number of surprising effects were obtained by BDMPS and Zakharov. First, the partonic energy loss in a hot QCD plasma is predicted to be much larger than in cold matter. This suggests that an anomalously large energy loss of jets produced in relativistic heavy-ion collisions could be a signature for Quark-Gluon Plasma formation. Second, the radiative energy loss is predicted to be proportional to  $L^2$ , where  $L$  is the path length of hot or cold nuclear matter traversed by the partons. This curious result is contrary to the conventional wisdom that energy loss depends linearly on  $L$ , and it reflects the quantum-mechanical interference effect from several contributing diagrams.

An attempt to search for partonic energy-loss effects in cold matter was made recently via the study of nuclear dependence of Drell-Yan cross sections at 800 GeV [18]. Only an upper limit for partonic energy loss was determined. A much more sensitive study can be made at lower beam energies, where the fractional energy loss  $\Delta E/E$  will be larger. At the 50-GeV PS, the effect is expected to be much enhanced and indeed one could even examine whether the nuclear effect follows the  $L$  or  $L^2$  dependence.

While logarithmic scaling violation is well established in DIS experiments, no clear evidence for scaling violation has been seen in Drell-Yan process. The 50-GeV PS provides an interesting opportunity for unambiguously establishing scaling violation in the Drell-Yan process [19]. For given values of  $x_1$  and  $x_2$  (Bjorken- $x$  for the projectile and target partons, respectively), scaling-violation is expected to cause roughly a factor of two increase in the Drell-Yan cross sections when proton beam energy is decreased from 800 GeV to 50 GeV. It appears quite feasible to establish scaling violation in the Drell-Yan process with future data from the 50-GeV PS.

Detection of high-mass dileptons at the 50-GeV PS will also allow a study of  $J/\Psi$  and  $\Psi'$  production. Existing data on proton-induced charmonium production are mostly limited to the energy range  $150 \text{ GeV} \leq E_p \leq 800 \text{ GeV}$ . A comparison of 50 GeV charmonium production data with existing data will further improve our knowledge on the production and propagation of charmonium in the nuclear medium. Many different effects which could affect the production of charmonium in nuclear medium, such as nuclear shadowing, partonic energy loss, final-state interaction with comoving gluons or hadrons, will have different beam energy dependences [20, 21]. Therefore, a systematic study of charmonium production in  $p - p$ ,  $p - A$  and  $A - A$  collisions at 50 GeV would be extremely valuable for disentangling various effects. Only after the mechanisms for charmonium production are well understood could  $J/\Psi$ -suppression be used confidently as a signature for Quark-

Gluon Plasma formation in relativistic heavy-ion collisions [22, 23].

Many of the proposed studies for Drell-Yan process at the 50-GeV PS could also benefit from the  $J/\Psi$  and  $\Psi'$  data. Unlike the Drell-Yan which is an electromagnetic process, quarkonium production is a strong-interaction process involving gluon-gluon fusion and quark-antiquark fusion. Comparison between the Drell-Yan and quarkonium production data will further elucidate various aspects of parton distributions in nucleons and nuclei, and of the propagation of partons in nuclei. As an example, charmonium production with polarized proton beam at the 50-GeV PS might provide interesting information on the gluon distributions at large Bjorken- $x$ , which is essentially unknown.

In this paper, we discuss the physics interest and the feasibility for making precise measurements of high-mass dimuons at the 50-GeV PS. In Section 2 the physics motivation for various measurements will be discussed in some details. A preliminary design study of a dimuon spectrometer for the 50-GeV PS will be presented in Section 3. A summary is given in Section 4.

## 2 Physics Issues

### 2.1 Overview of high-mass dilepton production

Detection of high-mass dileptons produced in high-energy hadronic interactions has a long and glorious history. The charm and beauty quarks were discovered in the 1970's via the dilepton decay modes of  $J/\Psi$  and  $\Upsilon$  resonances. These quarkonium states are superimposed on a dilepton continuum known as the Drell-Yan process [6]. The Drell-Yan data has been a source of information for the antiquark structure of the nucleon [24]. Furthermore, Drell-Yan production with pion and kaon beams has yielded the parton distributions of these unstable particles for the first time. A generalized Drell-Yan process was also responsible for the discovery of the  $W$  and  $Z$  gauge bosons in the 1980's.

To lowest order, the Drell-Yan process depends on the product of quark and antiquark distributions in the beam and target as

$$\frac{d^2\sigma}{dx_1 dx_2} = \frac{4\pi\alpha^2}{9s} \sum_a e_a^2 [q_a(x_1)\bar{q}_a(x_2) + \bar{q}_a(x_1)q_a(x_2)]. \quad (1)$$

Here  $q_a(x)$  are the quark or antiquark structure functions of the two colliding hadrons evaluated at momentum fractions  $x_1$  and  $x_2$ . The sum is over quark flavors, and  $s$  is the center-of-mass energy squared.

The kinematics of the virtual photon – longitudinal center-of-mass momentum  $p_{\parallel}^{\gamma}$ , transverse momentum  $p_T^{\gamma}$  and mass  $M_{\gamma}$  – are determined by measuring the two-muon decay of the virtual photon. These quantities determine the momentum fractions of the

two quarks:

$$x_F = p_{\parallel}^{\gamma} / p_{\parallel}^{\gamma, \max} = x_1 - x_2 \quad (2)$$

$$M_{\gamma}^2 = x_1 x_2 s \quad (3)$$

where  $p_{\parallel}^{\gamma}$  is the virtual photon center-of-mass longitudinal momentum and  $p_{\parallel}^{\gamma, \max}$  is the maximum value it can have.

Although the simple parton model enjoyed considerable success in explaining many features of the early data, it was soon realized that QCD corrections to the parton model were required. The inclusion of the NLO diagrams for the Drell-Yan process brings excellent agreement between the calculations and the data. As an example, Figure 1 shows the NA3 data [25] at 400 GeV, together with the E605 [26] and E772 [27] data at 800 GeV. The solid curves in Figure 1 correspond to NLO calculation for 800 GeV  $p + d$  ( $\sqrt{s} = 38.9$  GeV) and they describe the NA3/E605/E772 data well. This shows that the mechanism for Drell-Yan process is well understood theoretically, and quantitative information on the parton distributions can be reliably extracted via this process.

To gain sensitivity to the antiquark distribution of the target, one chooses a proton beam and selects the kinematic region of positive  $x_F$  and large  $x_1$ . In this limit the contribution from the second term in Eq. 1 is small and the first term is dominated by the  $u(x_1)$  distribution of the proton. Under these circumstances, the ratio of the cross sections for two different targets,  $X$  and  $Y$ , which have  $A_X$  and  $A_Y$  nucleons is approximately the ratio of the  $\bar{u}(x_2)$  distributions:

$$\frac{\frac{1}{A_X} \left( \frac{d\sigma^X}{dx_1 dx_2} \right)}{\frac{1}{A_Y} \left( \frac{d\sigma^Y}{dx_1 dx_2} \right)} \approx \frac{\bar{u}^X(x_2)}{\bar{u}^Y(x_2)} \Big|_{x_1 \gg x_2} \quad (4)$$

In this relation the cross sections are defined per nucleus but the parton distributions are conventionally defined per nucleon.

Eq. 4 demonstrates the power of Drell-Yan experiments in determining relative antiquark distributions. This feature was explored by recent Fermilab experiments using 800 GeV proton beams [7]. The 50-GeV PS provides a unique opportunity for extending the Fermilab measurements to larger  $x_2$  ( $x_2 > 0.25$ ). For a given value of  $x_1$  and  $x_2$ , the Drell-Yan cross section is proportional to  $1/s$  (see Eq. 1). Hence the cross section at 50 GeV is roughly 16 times greater than that at 800 GeV (The price one pays at lower beam energies is that one has limited reach for small  $x_2$ , which could best be studied at higher energies). Furthermore, to the extent that the radiation dose scales as beam power, one can take  $\approx 16$  times higher beam flux at 50 GeV relative to 800 GeV. The combination of these two effects could lead to two orders of magnitude improvement in the statistics at high  $x_2$  over previous Fermilab experiments.

## 2.2 Scaling violation in Drell-Yan process

The right-hand side of Eq. 1 is only a function of  $x_1, x_2$  and is independent of the beam energy. This scaling property no longer holds when QCD corrections to the Drell-Yan process are taken into account. While scaling violation is well established in DIS experiments, it is not confirmed in Drell-Yan experiments at all. No convincing evidence for scaling violation is seen [29]. As discussed in a recent review [7], there are mainly two reasons for this. First, unlike the DIS, the Drell-Yan cross section is a convolution of two structure functions. For proton-induced Drell-Yan, one often involves a beam quark with  $x_1 > 0.1$  and a target antiquark with  $x_2 < 0.1$ . Scaling violation implies that the structure functions rise for  $x \leq 0.1$  and drop for  $x \geq 0.1$  as  $Q^2$  increases. Hence the effects of scaling violation are partially cancelled. Second, unlike the DIS, the Drell-Yan experiment can only probe relatively large  $Q^2$ , namely,  $Q^2 > 16 \text{ GeV}^2$  for a mass cut of 4 GeV. This makes it more difficult to observe the logarithmic  $Q^2$  variation of the structure functions in Drell-Yan experiments.

The 50-GeV PS provides an interesting opportunity for unambiguously establishing scaling violation in the Drell-Yan process. Figure 2 shows the predictions for  $p + d$  at 50 GeV. Scaling violation causes a factor of two increase in the Drell-Yan cross sections when the beam energy is decreased from 800 GeV to 50 GeV. It appears quite feasible to establish scaling violation in Drell-Yan with future dilepton production experiments at the 50-GeV PS.

## 2.3 $\bar{d}/\bar{u}$ asymmetry of the proton

From neutrino-induced DIS experiments, it is known that the strange quark sea in the nucleon is roughly a factor of two less than the up or down quark sea [31]. The lack of SU(3) flavor symmetry in the nucleon sea is attributed to the much heavier mass of the strange quark. Until recently, it had been assumed that the distributions of  $\bar{u}$  and  $\bar{d}$  quarks were identical. Although the equality of  $\bar{u}$  and  $\bar{d}$  in the proton is not required by any known symmetry, this is a plausible assumption for sea quarks generated by gluon splitting. Because the masses of the up and down quarks are small compared to the confinement scale, nearly equal numbers of up and down sea quarks should result.

The assumption of  $\bar{u}(x) = \bar{d}(x)$  can be tested by measurements of the Gottfried integral [5], defined as

$$I_G = \int_0^1 [F_2^p(x, Q^2) - F_2^n(x, Q^2)] / x \, dx = \frac{1}{3} + \frac{2}{3} \int_0^1 [\bar{u}_p(x) - \bar{d}_p(x)] \, dx, \quad (5)$$

where  $F_2^p$  and  $F_2^n$  are the proton and neutron structure functions measured in DIS experiments. Under the assumption of a symmetric sea,  $\bar{u} = \bar{d}$ , the Gottfried Sum Rule (GSR) [5],  $I_G = 1/3$ , is obtained. The most accurate test of the GSR was reported in

1991 by the New Muon Collaboration (NMC) [4], which measured  $F_2^p$  and  $F_2^n$  over the region  $0.004 \leq x \leq 0.8$ . They determined the Gottfried integral to be  $0.235 \pm 0.026$ , significantly below  $1/3$ . This surprising result has generated much interest, and it strongly suggested that the assumption  $\bar{u} = \bar{d}$  should be abandoned. Specifically, the NMC result implies

$$\int_0^1 [\bar{d}(x) - \bar{u}(x)] dx = 0.148 \pm 0.039. \quad (6)$$

Eq. 6 shows that only the integral of  $\bar{d} - \bar{u}$  was deduced from the DIS measurements. The  $x$  dependence of  $\bar{d} - \bar{u}$  remained unspecified.

The proton-induced Drell-Yan process provides an independent means to probe the flavor asymmetry of the nucleon sea [32]. An important advantage of the Drell-Yan process is that the  $x$  dependence of  $\bar{d}/\bar{u}$  can be determined. The Fermilab E772 collaboration [33] compared the Drell-Yan yields from isoscalar targets with that from a neutron-rich (tungsten) target, and constraints on the nonequality of  $\bar{u}$  and  $\bar{d}$  in the range  $0.04 \leq x \leq 0.27$  were set. More recently, the CERN experiment NA51 [34] carried out a comparison of the Drell-Yan muon pair yield from hydrogen and deuterium using a 450 GeV/c proton beam. They found that  $\bar{u}/\bar{d} = 0.51 \pm 0.04 \pm 0.05$  at  $\langle x \rangle = 0.18$ , a surprisingly large difference between the  $\bar{u}$  and  $\bar{d}$ .

A Drell-Yan experiment (E866), aiming at higher statistical accuracy and wider kinematic coverage than NA51, was recently completed [8, 9] at Fermilab. This experiment also measured the Drell-Yan muon pairs from 800-GeV/c protons interacting with liquid deuterium and hydrogen targets. Eq. 4 shows that the Drell-Yan cross section ratio at large  $x_F$  is approximately given as

$$\frac{\sigma_{DY}(p+d)}{2\sigma_{DY}(p+p)} \approx \frac{1}{2} \left( 1 + \frac{\bar{d}(x_2)}{\bar{u}(x_2)} \right). \quad (7)$$

Values for  $\bar{d}/\bar{u}$  were extracted by the E866 collaboration at  $Q^2 = 54$  GeV $^2/c^2$  over the region  $0.02 < x < 0.345$ . These are shown in Figure 3 along with the NA51 measurement. For  $x < 0.15$ ,  $\bar{d}/\bar{u}$  increases linearly with  $x$  and is in good agreement with the CTEQ4M [28] and MRS(R2) [35] parameterizations. However, a distinct feature of the data, not seen in either parameterization, is the rapid decrease toward unity of  $\bar{d}/\bar{u}$  beyond  $x = 0.2$ .

The  $\bar{d}/\bar{u}$  ratio, along with the CTEQ4M values for  $\bar{d} + \bar{u}$ , was used to obtain  $\bar{d} - \bar{u}$  (Figure 4). Being a flavor nonsinglet quantity,  $\bar{d}(x) - \bar{u}(x)$  is decoupled from gluon distribution. Since perturbative processes have negligible contribution to  $\bar{d}/\bar{u}$  asymmetry,  $\bar{d}(x) - \bar{u}(x)$  essentially isolates the contribution from non-perturbative effects. From the results shown in Figure 4, one can obtain an independent determination [9] of the integral of Eq. 6. E866 finds  $0.100 \pm 0.007 \pm 0.017$ , consistent with, but roughly  $2/3$  of the value deduced by NMC.

As early as 1983, Thomas [36] pointed out that the virtual pions that dress the proton will lead to an enhancement of  $\bar{d}$  relative to  $\bar{u}$  via the (nonperturbative) “Sullivan process.” Sullivan [37] previously showed that in DIS virtual mesons scale in the Bjorken limit and contribute to the nucleon structure function. Following the publication of the NMC result, many papers treated virtual mesons as the origin of the  $\bar{d}/\bar{u}$  asymmetry (see [38] for a recent review). Here the  $\pi^+(\bar{d}u)$  cloud, dominant in the process  $p \rightarrow \pi^+ n$ , leads to an excess of  $\bar{d}$  sea.

A different approach for including the effects of virtual mesons has been presented by Eichten et al. [39] and further investigated by other authors [40, 41]. In chiral perturbation theory, the relevant degrees of freedom are constituent quarks, gluons, and Goldstone bosons. In this model, a portion of the sea comes from the couplings of Goldstone bosons to the constituent quarks, such as  $u \rightarrow d\pi^+$  and  $d \rightarrow u\pi^-$ . The excess of  $\bar{d}$  over  $\bar{u}$  is then simply due to the additional valence  $u$  quark in the proton.

The  $x$  dependence of  $\bar{d} - \bar{u}$  and  $\bar{d}/\bar{u}$  obtained by E866 provides important constraints for theoretical models. Figure 4 compares  $\bar{d}(x) - \bar{u}(x)$  from E866 with a virtual-pion model calculation, following the procedure detailed by Kumano [43]. A dipole form, with  $\Lambda = 1.0$  GeV for the  $\pi NN$  form factor and  $\Lambda = 0.8$  GeV for the  $\pi N\Delta$  form factor, was used.  $\Lambda$  is the cutoff parameter for the pion form factor. Figure 4 also shows the predicted  $\bar{d} - \bar{u}$  from the chiral model [41]. The chiral model places more strength at low  $x$  than does the virtual-pion model. This difference reflects the fact that the pions are softer in the chiral model, since they are coupled to constituent quarks that carry only a fraction of the nucleon momentum. The  $x$  dependence of the E866 data favors the virtual-pion model over the chiral model, suggesting that correlations between the chiral constituents should be taken into account.

Recently, the flavor asymmetry of the nucleon sea was computed in the large- $N_c$  limit, where the nucleon is described as a soliton of an effective chiral theory [12, 44]. In this chiral quark-soliton model, the flavor non-singlet distribution,  $\bar{d}(x) - \bar{u}(x)$ , appears in the next-to-leading order of the  $1/N_c$  expansion [11]. The E866  $\bar{d}(x) - \bar{u}(x)$  data were shown to be well described by this model [44].

Instantons have been known as theoretical constructs since the seventies [45, 46, 47]. They represent non-perturbative fluctuations of the gauge fields that induce transitions between degenerate ground states of different topology. In the case of QCD, the collision between a quark and an instanton flips the helicity of the quark while creating a  $q\bar{q}$  pair of different flavor. Thus, interaction between a  $u$  quark and an instanton results in a  $u$  quark of opposite helicity and either a  $d\bar{d}$  or  $s\bar{s}$  pair. Such a model has the possibility of accounting for both the flavor asymmetry and the “spin crisis” [48, 49]. However, the prediction [50] at large  $x$ ,  $\bar{d}(x)/\bar{u}(x) \rightarrow 4$ , is grossly violated by experiment (see Figure 3). Thus, it appears that while instantons have the possibility for accounting for flavor and spin anomalies, the approach is not yet sufficiently developed for a direct comparison.

The interplay between the perturbative and non-perturbative components of the nucleon sea remains to be better determined. Since the perturbative process gives a symmetric  $\bar{d}/\bar{u}$  while a non-perturbative process is needed to generate an asymmetric  $\bar{d}/\bar{u}$  sea, the relative importance of these two components is directly reflected in the  $\bar{d}/\bar{u}$  ratios. Thus, it would be very important to extend the Drell-Yan measurements to kinematic regimes beyond the current limits.

The 50-GeV PS presents an excellent opportunity for extending the  $\bar{d}/\bar{u}$  measurement to larger  $x$  ( $x > 0.25$ ). As mentioned earlier, for given values of  $x_1$  and  $x_2$  the Drell-Yan cross section is proportional to  $1/s$ , hence the Drell-Yan cross section at 50 GeV is roughly 16 times greater than at 800 GeV. Figure 5 shows the expected statistical accuracy for  $\sigma(p+d)/2\sigma(p+p)$  at the 50-GeV PS (see Section 3) compared with the data from E866 and a proposed measurement [51] using the 120 GeV proton beam at the Fermilab Main-Injector. A definitive measurement of the  $\bar{d}/\bar{u}$  over the region  $0.25 < x < 0.7$  could indeed be obtained at the 50-GeV PS.

## 2.4 Polarized Drell-Yan at the 50-GeV PS

Despite extensive work on polarized DIS, the helicity distributions of  $\bar{u}$  and  $\bar{d}$  sea quarks are still poorly known. Both the SMC [52] and the HERMES [53] experiments attempted to extract the sea-quark polarizations via semi-inclusive polarized DIS measurements, and the results indicate small sea-quark polarization consistent with zero. However, as pointed out in Ref. [54], large uncertainties are associated with certain assumptions made in the extraction.

A direct measurement of sea-quark's polarization is clearly very important for understanding the flavor decomposition of proton's spin. Different theoretical models make drastically different predictions. In particular, the meson-cloud models, which successfully describe the unpolarized  $\bar{d}/\bar{u}$  asymmetry, predict negligible amount of sea-quark polarization [55, 56]. Several current parametrizations [57, 58] of polarized parton distributions also assume very small polarization for sea quarks. The chiral-quark soliton model, on the other hand, predicts substantial sea-quark polarization [11, 54]. Figure 6 shows  $x\Delta\bar{u}(x)$ ,  $x\Delta\bar{d}(x)$ , and  $x\Delta\bar{s}(x)$  at  $Q_0^2 = 0.36$  GeV $^2$  from a recent prediction of chiral-quark soliton model [59]. Also shown in Figure 6 are the GRSV parametrizations [58] from a global fit to polarized DIS data.

A very striking prediction of the chiral-quark model is the large flavor asymmetry of polarized sea-quark polarization. In fact, this model predicts a significantly larger values for  $\Delta\bar{u} - \Delta\bar{d}$  than for  $\bar{d} - \bar{u}$ . This is shown in Figure 7, where  $x(\Delta\bar{u} - \Delta\bar{d})$  from the chiral-quark soliton model [59] is compared with the  $x(\bar{d} - \bar{u})$  parametrization from GRV94 [60].

Polarized proton beam at the 50-GeV PS would offer an exciting opportunity for

probing sea-quark polarizations. The longitudinal spin asymmetry in the DY process is, in leading order, given by [61],

$$A_{LL}^{DY}(x_1, x_2) = \frac{\sum_a e_a^2 [\Delta q_a(x_1) \Delta \bar{q}_a(x_2) + \Delta \bar{q}_a(x_1) \Delta q_a(x_2)]}{\sum_a e_a^2 [q_a(x_1) \bar{q}_a(x_2) + \bar{q}_a(x_1) q_a(x_2)]}, \quad (8)$$

with  $\Delta q_a \equiv q_a^+ - q_a^-$ . The superscripts refer to parton spin projections parallel (+) or antiparallel (-) to the proton's spin projection. We have simulated the performance of the proposed high-mass dimuon spectrometer for measuring polarized antiquark distribution. Figure 8 shows the  $x_2$  dependence of  $A_{LL}^{DY}$ , integrated over the spectrometer acceptance, for polarized sea-quark parametrizations including Gehrmann-Stirling (G-S) sets A and C [57] and GRSV Leading-Order set [58]. Very small values for  $A_{LL}^{DY}$  are predicted for the G-S parametrization, while the GRSV parametrization gives  $A_{LL}^{DY} \approx -0.2$ . The chiral-quark soliton model gives large positive  $A_{LL}^{DY}$ . In fact, the positivity requirement, namely,  $-1 < \Delta \bar{u}(x)/\bar{u}(x) < 1$ , is not always satisfied at the region  $x > 0.2$  for the particular parametrization given by Ref. [59].

We have calculated the expected statistical sensitivities for a 120-day  $\vec{p} + \vec{p}$  measurement, assuming 75% polarization for a  $5 \times 10^{11}$  per spill polarized proton beam. We also assume a polarized solid NH<sub>3</sub> target similar to the one used by the SMC [62] which achieves a hydrogen polarization of 75% and a dilution factor of 0.15. The target length is chosen to give the same gm/cm<sup>2</sup> as for the liquid deuterium target. Figure 8 shows that the statistical accuracy of such a measurement can well test the predictions of various model (note that the chiral-quark soliton model predicts a large positive  $A_{LL}^{DY}$  not shown in this figure). A comparison of  $\vec{p} + \vec{p}$  with  $\vec{p} + \vec{d}$  will further determine  $\Delta \bar{d}$ , which provides a direct test of the chiral-quark soliton model's prediction of large  $\Delta \bar{u} - \Delta \bar{d}$ .

In the polarized Drell-Yan process one may also measure a new structure function, called transversity, which is a correlation between quark momentum and its perpendicular spin component [63]. The transversity is not measurable in inclusive DIS [64]. It is measurable, in principle, in collisions of polarized protons whose spins are aligned perpendicular to the plane of dilepton detection [65]. A non-zero transverse spin correlation in the Drell-Yan process would clearly require both quark and antiquark transversities to be non-zero. Polarized proton beam at the 50-GeV PS could provide unique information on the transversities at large  $x$ .

## 2.5 Nuclear effects of Drell-Yan

Following the discovery of the EMC effect, it was suggested [66, 67, 68] that this effect is caused by the excess of virtual pions in nuclei, which significantly modify the nuclear parton distributions. A direct consequence of the “pion-excess” model is the nuclear enhancement of antiquark sea, which can be probed via Drell-Yan experiment [69]. However, the subsequent Fermilab E772 experiment [10] found no evidence for such enhancement (see Figure 9). The lack of an antiquark enhancement in nuclei suggests that there are

no more pions surrounding an average nucleon in a heavy nucleus than there are in a weakly bound system, deuterium. This contradicts conventional wisdom and is also at odds with sophisticated calculations using realistic nuclear force [70]. Unfortunately, the error bars for the E772 data in the region  $x > 0.15$  become quite large, due entirely to limited statistics. Furthermore, at  $x < 0.1$  the on-set of the shadowing effect makes the isolation of possible pion-excess effect somewhat uncertain.

At the 50-GeV PS, one can measure the nuclear effect over the large  $x$  region ( $x > 0.15$ ) with high accuracy. This is illustrated in Figure 9, where the expected statistical errors for a 60-day measurement of  $p+Ca$  and  $p+d$  using the proposed spectrometer (see Section 3) are shown. One advantage of the 50-GeV measurement is that shadowing effect is no longer important at large  $x$ . The precise measurement at  $x$  larger than E772 could access would provide extremely valuable new information on the nuclear dependence of antiquark distributions. The anticipated sensitivity will be sufficient to observe the reduction in the nuclear sea distributions predicted in the  $Q^2$  rescaling models [71]. The pion-excess model, on the other hand, predicts a strong nuclear enhancement of Drell-Yan cross sections in this  $x$  region.

## 2.6 Partonic energy loss in nuclei

The subject of energy loss of fast partons propagating through hadronic matters has attracted considerable interest recently [72]. The nuclear dependence of the Drell-Yan process provides a particularly clean way to measure the energy loss of incident quarks in a cold nuclear medium. Partonic energy loss would lead to a degradation of the quark momentum prior to annihilation, resulting in a less energetic muon pair. Therefore, one expects the Drell-Yan cross sections for heavier nuclear targets to drop more rapidly at large  $x_1$  (or  $x_F$ ).

Data from E772 at 800 GeV/c were analysed by Gavin and Milana [73] to deduce the initial-state quark energy loss. They ignored the shadowing effect and assumed the following expression for the average change in the momentum fraction:

$$\Delta x_1 = -\kappa_1 x_1 A^{1/3}. \quad (9)$$

A surprisingly large fractional energy loss ( $\approx 0.4\% / fm$ ) was obtained. This result was questioned by Brodsky and Hoyer [74], who argued that the time scale for gluon bremsstrahlung need to be taken into account. Moreover, as pointed out in Ref. [7], it is important to account for the shadowing effect before a reliable value of partonic energy loss can be extracted. Using an analogy to the photon bremsstrahlung process, Brodsky and Hoyer suggested an alternative expression:

$$\Delta x_1 \approx -\frac{\kappa_2}{s} A^{1/3}, \quad (10)$$

where  $s$  is the square of the nucleon-nucleon center-of-mass energy. Note that Eq. 9 implies a linear dependence of the energy loss on the partonic energy, while Eq. 10 assumes

a constant energy loss independent of the partonic energy (note that  $\Delta E$  is proportional to  $\Delta x_1 s$ ). Based on uncertainty principle, Brodsky and Hoyer concluded that energetic partons should loose  $\leq 0.5$  GeV/fm in nuclei. More recently, Baier et al. [13] and Zakharov [14] predicted

$$\Delta x_1 \approx -\frac{\kappa_3}{s} A^{2/3}. \quad (11)$$

These authors obtained the nonintuitive result that the total energy loss is proportional to the square of the path length traversed.

Very recently, the E866 nuclear-dependence data have been analysed by taking into consideration the shadowing effect and comparing with the three different expressions (Eqs. 9 - 11) for energy loss [18]. Upper limits of  $\kappa_2 < 0.75$  GeV<sup>2</sup> and  $\kappa_3 < 0.10$  GeV<sup>2</sup> have been obtained. The  $\kappa_2$  limit corresponds to a constant energy loss rate of  $< 0.44$  GeV/fm, while the  $\kappa_3$  limit implies  $\Delta E < 0.046$  GeV/fm<sup>2</sup>  $\times L^2$ , where  $L$  is the quark propagation length through the nucleus. This is very close to the lower value given by Baier et al. [13] for cold nuclear matter.

A much more sensitive study of the partonic energy loss could be carried out at the 50-GeV PS. We have simulated the effect of initial-state energy loss on the  $p + W$  Drell-Yan cross sections, and the results are shown in Figure 10. Assuming a 60-day run with the nominal spectrometer configuration (see Section 3), the expected  $x_1$  distribution for  $p + d$  is shown as the solid curve. The dashed, dotted, and dash-dotted curves in Figure 10 correspond to  $p + W$   $x_1$  spectra assuming a partonic energy loss form of Eq. 10 with  $dE/dz$  of -0.1, -0.25, -0.5 GeV/fm, respectively. The ratios of  $p + W$  over  $p + d$ , shown in Figure 10, are very sensitive to the quark energy loss rate, and the expected statistical accuracy can easily identify an energy loss as small as 0.1 GeV/fm. The greater sensitivity at 50 GeV is due to the  $1/s$  factor in Eq. 10 and Eq. 11. Another important advantage at 50 GeV is the absence of shadowing effect, and no shadowing correction is required.

The Drell-Yan A-dependence data could further be used to determine whether the energy loss follows an  $L$  (as in Eq. 10) or an  $L^2$  (as in Eq. 11) dependence. This is illustrated in Figure 11, where the solid circles correspond to  $(p + A)/(p + d)$  assuming an energy-loss rate of 0.25 GeV/fm using Eq. 10. The open squares correspond to the situation when energy loss is described by Eq. 11 (the value of  $\kappa_3$  is selected by matching the  $(p + W)/(p + d)$  values for both cases). Figure 11 shows that one can easily distinguish an  $L$ - from an  $L^2$ -dependence even when the energy loss rate is as small as 0.25 GeV/fm.

## 2.7 Quarkonium Production at 50 GeV

Unlike the Drell-Yan process, the mechanisms for  $J/\Psi$  production are not well understood. Several quarkonium production models have been considered in the literature, including color-evaporation, color-singlet, and color-octet models. For simplicity, we consider the

color-evaporation model, which is capable of describing the energy-dependence and the shape of the differential cross sections well. However, the absolute normalization of this model is treated as a parameter.

Figure 12 shows the prediction of the color-evaporation model for  $J/\Psi$  production at 50 GeV. The absolute normalization is obtained from an extrapolation of the global fit of existing  $J/\Psi$  data [75]. Unlike the situation at 800 GeV where the gluon-gluon fusion subprocess dominates [76], Figure 12 shows that the quark-antiquark annihilation is the dominant subprocess at 50 GeV. While this is reminiscent of the Drell-Yan process, it is worth noting that quarkonium production is a hadronic process unlike the electromagnetic Drell-Yan process. Hence, there is no  $e_q^2$  weighting factor for the  $q - \bar{q}$  subprocess in  $J/\Psi$  production.

As indicated in Figure 12, the  $J/\Psi$  production data at 50 GeV are largely sensitive to quark distributions and could provide information similar to Drell-Yan. This is illustrated in Figure 13 which shows that the  $J/\Psi$  cross section ratio for  $p + d$  over  $p + p$  is very sensitive to the  $\bar{d}/\bar{u}$  asymmetry just like the Drell-Yan process. This could be readily tested at the 50-GeV PS, since the  $J/\Psi$  event rate is expected to be very high.

It is also of interest to measure  $J/\Psi$  production using polarized proton beam and target. Unfortunately, the uncertainty of the production mechanism might make it difficult to deduce information on polarized structure functions.

### 3 Experimental Apparatus

The spectrometer considered here is designed to measure muon pairs at  $M_{\mu^+\mu^-} \geq 1$  GeV with 50 GeV proton beam. The E866 spectrometer and its daughter, a proposed P906 spectrometer [51], are taken as a starting point. The E866 spectrometer is shown in Figure 14.  $\mu^+\mu^-$  pairs produced at the target were analyzed by a vertical-bending spectrometer. The remaining proton beam was intercepted by a copper beam dump located inside the dipole magnet. The beam dump was followed by a set of absorbers made of copper, carbon, and polyethylene, which absorbed many of the pions and kaons produced at the target before they could decay into muon backgrounds. Trigger hodoscopes, muon identifiers, and tracking counters followed the magnets. The magnetic current can be adjusted to optimize the acceptance of a selected mass range. The spectrometer has good acceptance for dimuons with  $x_F > 0$  and  $p_T$  up to 3 GeV/c.

To design a spectrometer suitable for 50 GeV proton beam, it is useful to consider some kinematics of the Drell-Yan process. Table 1 compares the total center-of-mass energy and the Lorentz factor for proton beams of 50 GeV (at the present project), 120 GeV (at Fermilab Main Injector) and 800 GeV (at Fermilab Tevatron).

Table 1: The center-of-mass energy and the Lorentz factor for three beam energies

	50 GeV	120 GeV	800 GeV
$\sqrt{s}$	9.865 GeV	15.12 GeV	38.79 GeV
$\gamma_f$	5.259	7.998	20.65

The Lorentz factor of the nucleon-nucleon center-of-mass frame is

$$\gamma_f = \frac{E_1 + m_2}{\sqrt{s}}. \quad (12)$$

For  $\mu^+$  and  $\mu^-$  emitted at  $90^\circ$  in the nucleon-nucleon center-of-mass frame and for  $x_F \approx 0$ , the opening angle  $\theta$  of the two muons in the laboratory frame is expressed as

$$\tan(\theta/2) = \frac{1}{\gamma_f}. \quad (13)$$

For muons emitted at  $90^\circ$  in the virtual-photon rest frame, the laboratory kinematics of the muons largely depends on  $M$  and  $x_2$  and does not depend on beam energy (or  $\sqrt{s}$ ). More specifically,

$$p_\perp^{lab} = M/2. \quad (14)$$

$$p_\parallel^{lab} = \frac{1}{2} p_\parallel^{\gamma,lab} \simeq \frac{1}{2} x_1 p^{beam} \simeq \frac{x_1 s}{4m_N} = \frac{M^2}{2x_2 m_N}. \quad (15)$$

The measurable  $p_t$  range of muons should be almost the same as the E866 spectrometer or slightly smaller because the mass ( $M_{\mu^+\mu^-}$ ) range interested is the same or slightly less. Thus the total magnetic rigidity ( $\int B dl$ ) of the magnets should be about 7 to 10 T·m, though it depends on the geometrical layout of the detectors. The P906 spectrometer has a magnetic rigidity of 8 T·m.

According to Eq. 13, the opening angle of the muons at 50 GeV is about 4 times larger than at 800 GeV (E866), and 1.5 times larger than at 120 GeV (P906). One idea to design the 50-GeV spectrometer is just to shorten the existing setup in the beam (z) direction with the factor of  $\gamma(50 \text{ GeV})/\gamma(800 \text{ GeV})$  or  $\gamma(50 \text{ GeV})/\gamma(120 \text{ GeV})$ . However, since the maximum field strength of the P906 magnet is already near the saturation point, a magnet of almost the same length and wider aperture need to be considered.

Figure 15 shows the horizontal and vertical view of the proposed spectrometer. The target is assumed to be a liquid hydrogen or deuterium target 20-inch long and 3-inch wide. The produced charged particles are analyzed by a vertical-bending magnet, which is basically the same as the P906 magnet but has a wider aperture. The length of the magnet along the beam axis is 480.06 cm. The horizontal gap of the magnet at the exit is 116.84 cm and the vertical gap at the exit is 279.4 cm. The total momentum kick by this magnet is about 2.5 GeV/c. The incident proton beam is stopped by a copper beam dump, followed by a set of absorber materials. The second magnet and detectors are

placed after the first magnet. The momentum kick by the second magnet is 0.5 GeV/c. The total length of the spectrometer system from the entrance of the first magnet to the end of the detector system is 1474.47 cm. The muons which hit all the detectors are accepted as signals.

A fast Monte-Carlo code, which takes into account the Drell-Yan cross section and the spectrometer configuration, has been used to estimate a statistical error for  $\sigma(pd)/2\sigma(pp)$  shown in Figure 5. In order to estimate the yields and statistical errors, the following assumptions have been applied:

- The beam intensity is  $1 \times 10^{12}$  protons/(3 sec.).
- The net efficiency of data acquisition is 0.5.
- Data are taken for 60 days each for 50-cm long proton and deuteron targets.

The performance of the spectrometer for  $\vec{p} + \vec{p}$  measurement, nuclear dependence study of Drell-Yan, and  $J/\Psi$  production, has also been simulated and the results have been presented in the previous Section.

## 4 Summary

We present a broad range of physics topics which can be pursued at the 50-GeV PS using a dimuon spectrometer and a primary proton beam of  $10^{12}$  per spill. The expected sensitivities of various measurements have been simulated for a preliminary design of the dimuon spectrometer. The physics scope can be considerably enlarged with the addition of polarized proton beam and with heavy-ion beams. More detailed studies using GEANT-based simulation are in progress to address the issues of background and to optimize the design of the spectrometer. Based on our study thus far, it is clear that a rich physics program can be mounted using the primary proton beam at the 50-GeV PS.

## References

- [1] J. J. Aubert *et al.*, Phys. Lett. **B123**, 295 (1983).
- [2] D. F. Geesaman, K. Saito, A. W. Thomas, Annu. Rev. Nucl. Part. Sci. **45**, 337 (1995).
- [3] E. Hughes and R. Voss, Annu. Rev. Nucl. Part. Sci. **49**, 303 (1999).
- [4] P. Amaudruz *et al.*, Phys. Rev. Lett. **66**, 2712 (1991); M. Arneodo *et al.*, Phys. Rev. D **55**, R1 (1994).
- [5] K. Gottfried, Phys. Rev. Lett. **18**, 1174 (1967).
- [6] S. D. Drell and T. M. Yan, Phys. Rev. Lett. **25**, 316 (1971).
- [7] P. L. McGaughey, J. M. Moss and J. C. Peng, Annu. Rev. Nucl. Part. Sci. **49**, 217 (1999).
- [8] E. A. Hawker *et al.*, Phys. Rev. Lett. **80**, 3715 (1998).
- [9] J. C. Peng *et al.*, Phys. Rev. D **58**, 092004 (1998).
- [10] D. A. Alde *et al.*, Phys. Rev. Lett. **64**, 2479 (1990).
- [11] D. I. Diakonov *et al.*, Phys. Rev. D **56**, 4069 (1997).
- [12] M. Wakamatsu and T. Kubota, Phys. Rev. D **60**, 034020 (1999).
- [13] R. Baier *et al.*, Phys. Lett. **B345**, 277 (1995); Nucl. Phys. **B483**, 291 (1997); Nucl. Phys. **B484**, 265 (1997).
- [14] R. G. Zakharov, JETP Letters **63**, 952 (1996); JETP Letters **65**, 615 (1997).
- [15] L. D. Landau and I. Ya. Pomeranchuk, Dokl. Akad. Nauk SSSR **92**, 535 (1953); **92**, 735 (1953).
- [16] A. B. Migdal, Phys. Rev. **103**, 1811 (1956).
- [17] P. L. Anthony *et al.*, Phys. Rev. Lett. **75**, 1949 (1995); Phys. Rev. D **56**, 1373 (1997).
- [18] M. A. Vasiliev *et al.*, Phys. Rev. Lett. **83**, 2304 (1999).
- [19] J. C. Peng, hep-ph/9912371 (1999).
- [20] C. Gerschel and J. Hüfner, Annu. Rev. Nucl. Part. Sci. **49**, 255 (1999).
- [21] R. Vogt, Phys. Rev. C **61**, 035203 (2000).
- [22] T. Matsui and H. Satz, Phys. Lett. **B178**, 416 (1986).

- [23] M. C. Abreu *et al.*, CERN-EP-2000-013 (2000).
- [24] I. R. Kenyon, Rep. Prog. Phys. **45**, 1261 (1982).
- [25] J. Badier *et al.*, Z. Phys. **C26**, 489 (1984).
- [26] G. Moreno *et al.*, Phys. Rev. **D43**, 2815 (1991).
- [27] P. L. McGaughey *et al.*, Phys. Rev. **D50**, 3038 (1994).
- [28] H. L. Lai *et al.*, Phys. Rev. **D55**, 1280 (1997).
- [29] K. Freudenreich, Int. J. Mod. Phys. **A5**, 3643 (1990).
- [30] A. D. Martin *et al.*, Eur. Phys. J. **C4**, 463 (1998).
- [31] H. Abromowicz *et al.*, Z. Phys. **C15**, 19 (1982).
- [32] S. D. Ellis and W. J. Stirling, Phys. Lett. **B256**, 258 (1991).
- [33] P. L. McGaughey *et al.*, Phys. Rev. Lett. **69**, 1726 (1991).
- [34] A. Baldit *et al.*, Phys. Lett. **B332**, 244 (1994).
- [35] A. D. Martin, R. G. Roberts, W. J. Stirling, Phys. Lett. **B387**, 419 (1996).
- [36] A. W. Thomas, Phys. Lett. **B126**, 97 (1983).
- [37] J. D. Sullivan, Phys. Rev. **D5**, 1732 (1972).
- [38] S. Kumano, Phys. Rept. **303**, 183 (1998).
- [39] E. J. Eichten, I. Hinchliffe, C. Quigg, Phys. Rev. **D45**, 2269 (1992).
- [40] T. P. Cheng and L. F. Li, Phys. Rev. Lett. **74**, 2872 (1995).
- [41] A. Szczurek, A. Buchmans, A. Faessler, J. Phys. **C22**, 1741 (1996).
- [42] K. Ackerstaff *et al.*, Phys. Rev. Lett. **81**, 5519 (1998).
- [43] S. Kumano, Phys. Rev. **D43**, 3067 (1991); **D43**, 59 (1991); S. Kumano and J. T. Londergan, Phys. Rev. **D44**, 717 (1991).
- [44] P. V. Pobylitsa *et al.*, Phys. Rev. **D59**, 034024 (1999).
- [45] A. A. Belavin *et al.*, Phys. Lett. **B59**, 85 (1975).
- [46] G. t'Hooft, Phys. Rev. Lett. **37**, 8 (1976).
- [47] T. Schaefer and E. Shuryak, Rev. Mod. Phys. **70**, 323 (1998).

- [48] S. Forte, Phys. Lett. **B224**, 189 (1989).
- [49] S. Forte, Acta Phys. Polon. **B22**, 1065 (1991).
- [50] A. E. Dorokhov and N. I. Kochelev, Phys. Lett. **B259**, 335 (1991); **B335**, 167 (1993).
- [51] Proposal for Drell-Yan Measurements of Nucleon and Nuclear Structure with FNAL Main Injector, P906 Collaboration,  
[http://p25ext.lanl.gov/e866/papers/p906/proposal\\_final.ps](http://p25ext.lanl.gov/e866/papers/p906/proposal_final.ps).
- [52] B. Adeva *et al.*, Phys. Lett. **B420**, 180 (1998).
- [53] K. Ackerstaff *et al.*, hep-ex/9906035 (1999).
- [54] B. Dressler *et al.*, hep-ph/9909541 (1999).
- [55] R. J. Fries and A. Schäfer, Phys. Lett. **B443**, 40 (1998).
- [56] K. G. Boreskov and A. B. Kaidalov, Eur. Phys. J. **C10**, 143 (1999).
- [57] T. Gehrmann and W. J. Stirling, Phys. Rev. **D53**, 6100 (1996).
- [58] M. Glück, E. Reya, M. Stratmann and W. Vogelsang, Phys. Rev. **D53**, 4775 (1996).
- [59] K. Goeke *et al.*, hep-ph/0003324 (2000).
- [60] M. Glück, E. Reya and A. Vogt, Z. Phys. **C67**, 433 (1995).
- [61] F. E. Close and D. Sivers, Phys. Rev. Lett. **39**, 1116 (1977).
- [62] D. Adams *et al.*, Nucl. Instru. Meth. **A437**, 23 (1999).
- [63] J. Ralston and D. E. Soper, Nucl. Phys. **B152**, 109 (1979).
- [64] R. L. Jaffe and X. Ji, Phys. Rev. Lett. **67**, 552 (1991).
- [65] S. Kumano, hep-ph/0001053 (2000).
- [66] C. H. Llewellyn-Smith, Phys. Lett. **B128**, 107 (1983).
- [67] M. Ericson and A. W. Thomas, Phys. Lett. **B128**, 112 (1983).
- [68] E. L. Berger, F. Coester and R. B. Wiringa, Phys. Rev. **D29**, 398 (1984).
- [69] R. P. Bickerstaff *et al.*, Phys. Rev. Lett. **53**, 2531 (1984).
- [70] V. R. Pandharipande *et al.*, Phys. Rev. **C49**, 789 (1994); A. Akmal *et al.*, Phys. Rev. **C56**, 2261 (1997).
- [71] F. E. Close, R. L. Jaffe, R. G. Roberts and G. G. Ross, Phys. Rev. **D31**, 1004 (1985).

- [72] R. Baier, D. Schiff and B. G. Zakharov, hep-ph/0002198 (2000).
- [73] S. Gavin and J. Milana, Phys. Rev. Lett. **68**, 1834 (1992).
- [74] S. J. Brodsky and P. Hoyer, Phys. Lett. **B298**, 165 (1993).
- [75] M. H. Schub *et al.*, Phys. Rev. **D52**, 1307 (1995).
- [76] M. S. Kowitt *et al.*, Phys. Rev. Lett. **72**, 1318 (1994).



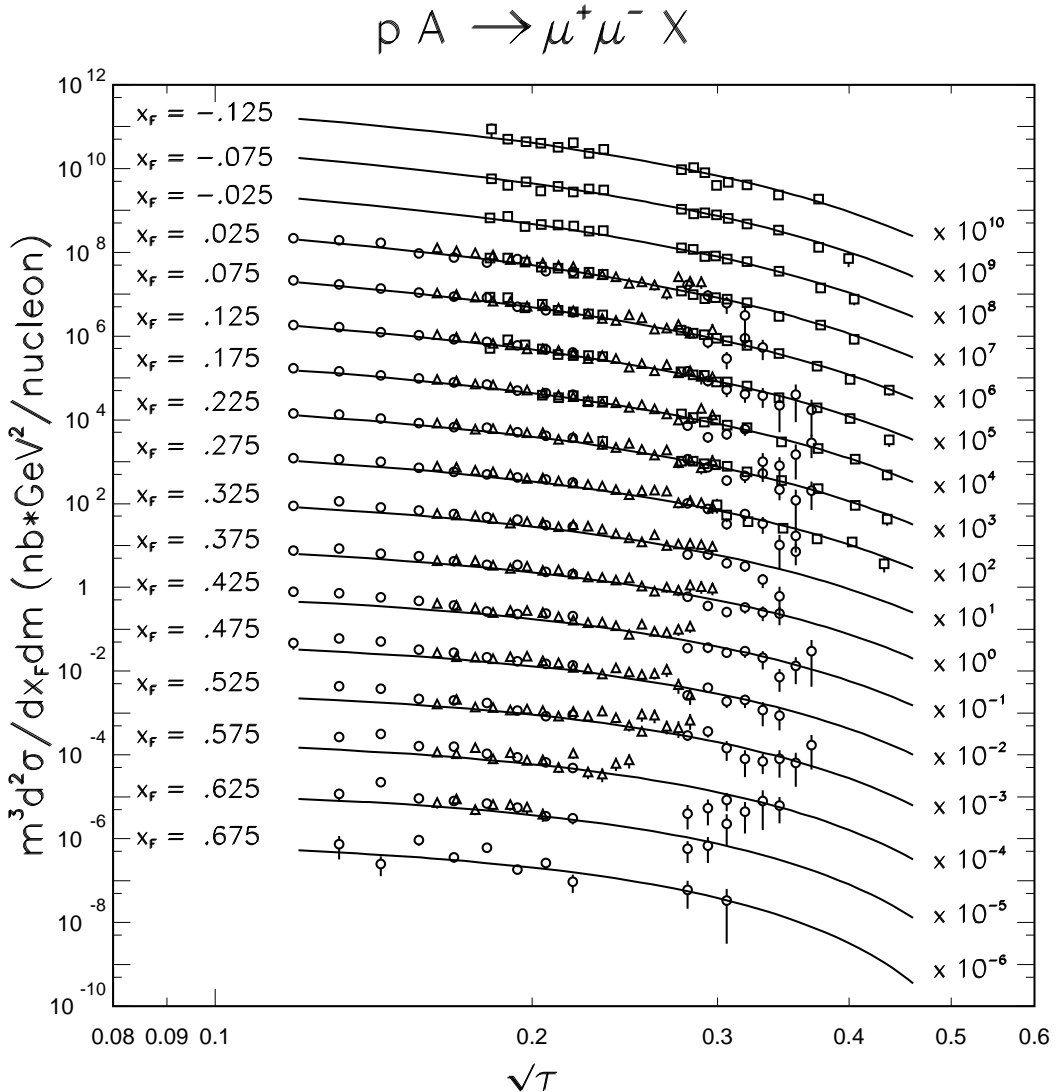


Figure 1: Proton-induced Drell-Yan production from experiments NA3 [25] (triangles) at 400 GeV/c, E605 [26] (squares) at 800 GeV/c, and E772 [27] (circles) at 800 GeV/c. The lines are absolute (no arbitrary normalization factor) next-to-leading order calculations for  $p + d$  collisions at 800 GeV/c using the CTEQ4M structure functions [28].

$p\ A \rightarrow \mu^+\mu^- X$

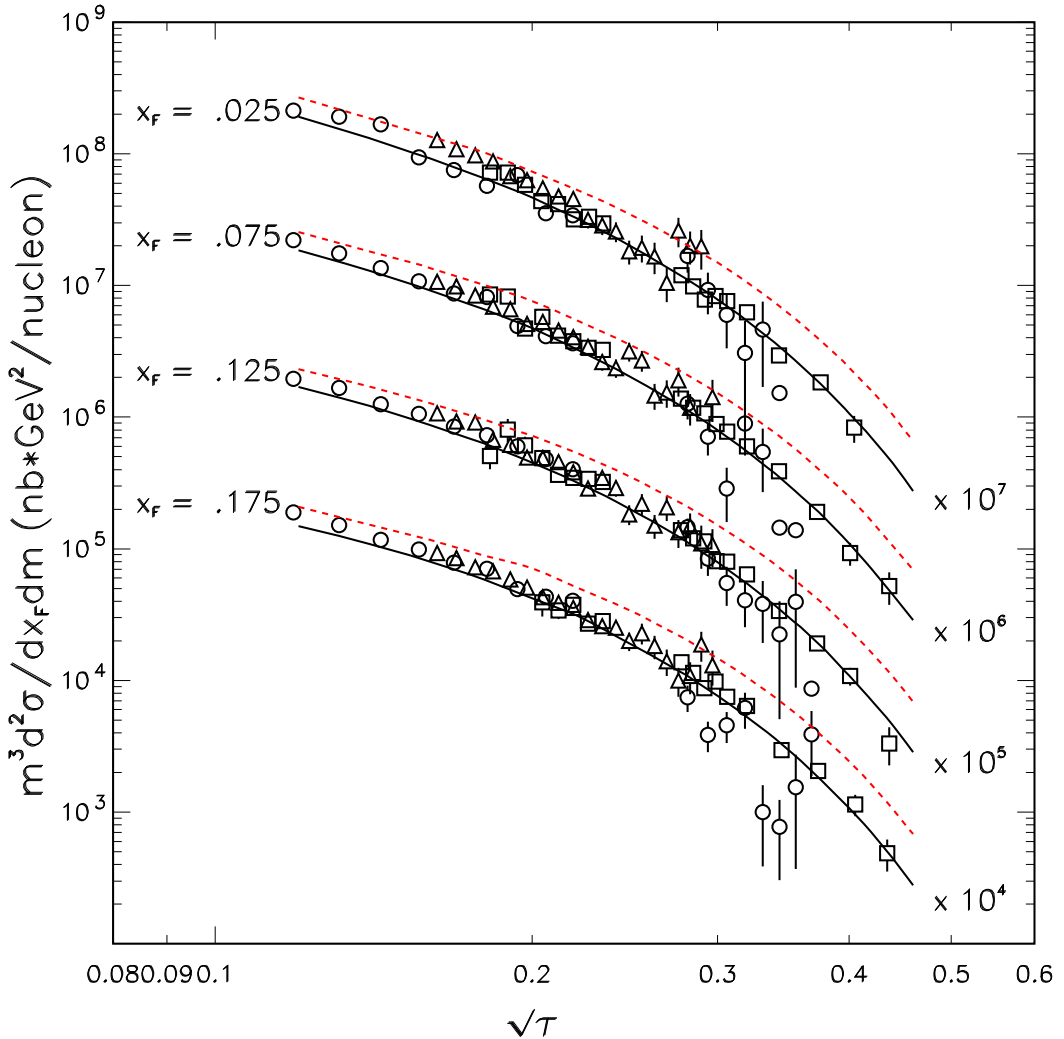


Figure 2: Comparison of Drell-Yan cross section data with NLO calculations using MRST [30] structure functions. Note that  $\tau = x_1 x_2$ . The E772 [27], E605 [26], and NA3 [25] data points are shown as circles, squares, and triangles, respectively. The solid curves correspond to fixed-target  $p + d$  collision at 800 GeV, while the dashed curve is for  $p + d$  collision at 50 GeV.

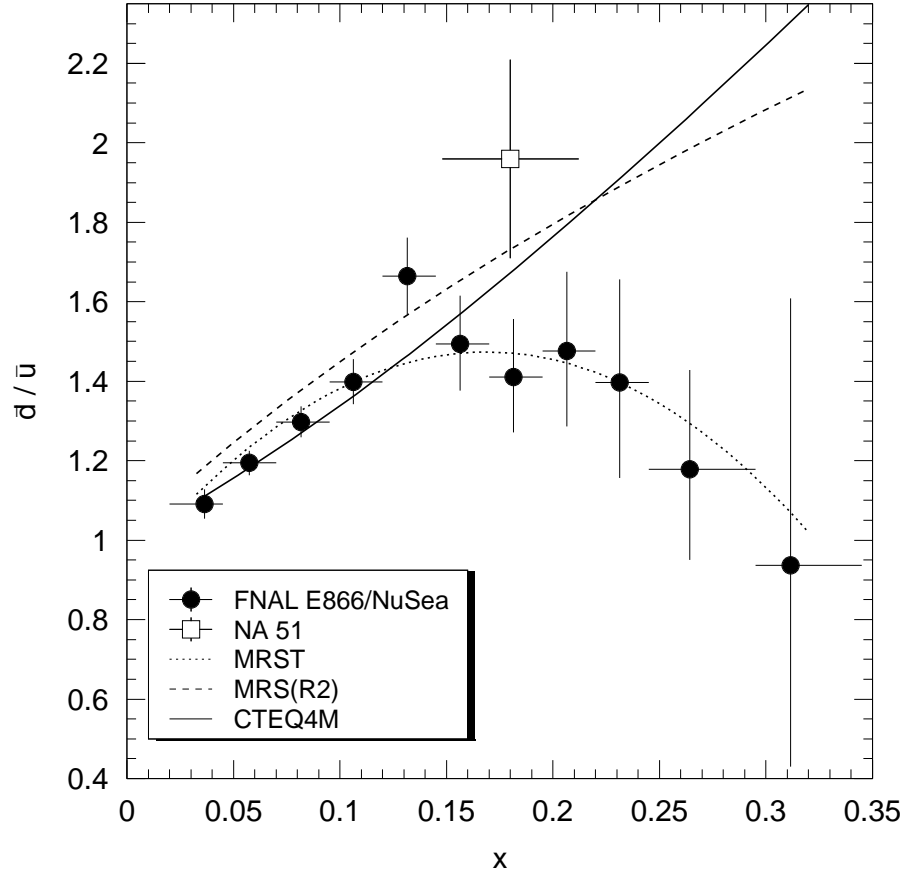


Figure 3: The ratio of  $\bar{d}/\bar{u}$  in the proton as a function of  $x$  extracted from the Fermilab E866 [8] cross section ratio. The curves are from various parton distributions. Also shown is the result from NA51 [34], plotted as an open square.

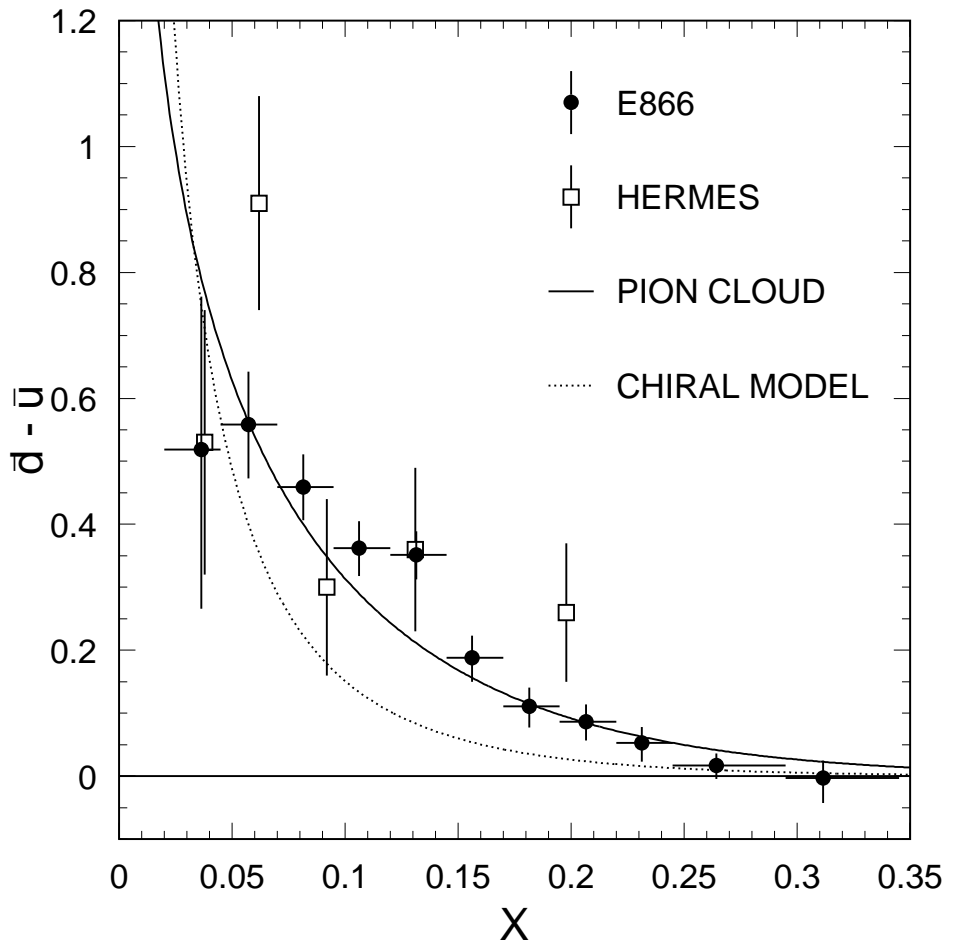


Figure 4: Comparison of the E866 [8]  $\bar{d} - \bar{u}$  results at  $Q^2 = 54 \text{ GeV}^2/\text{c}^2$  with the predictions of pion-cloud and chiral models as described in the text. The data from HERMES [42] are also shown.

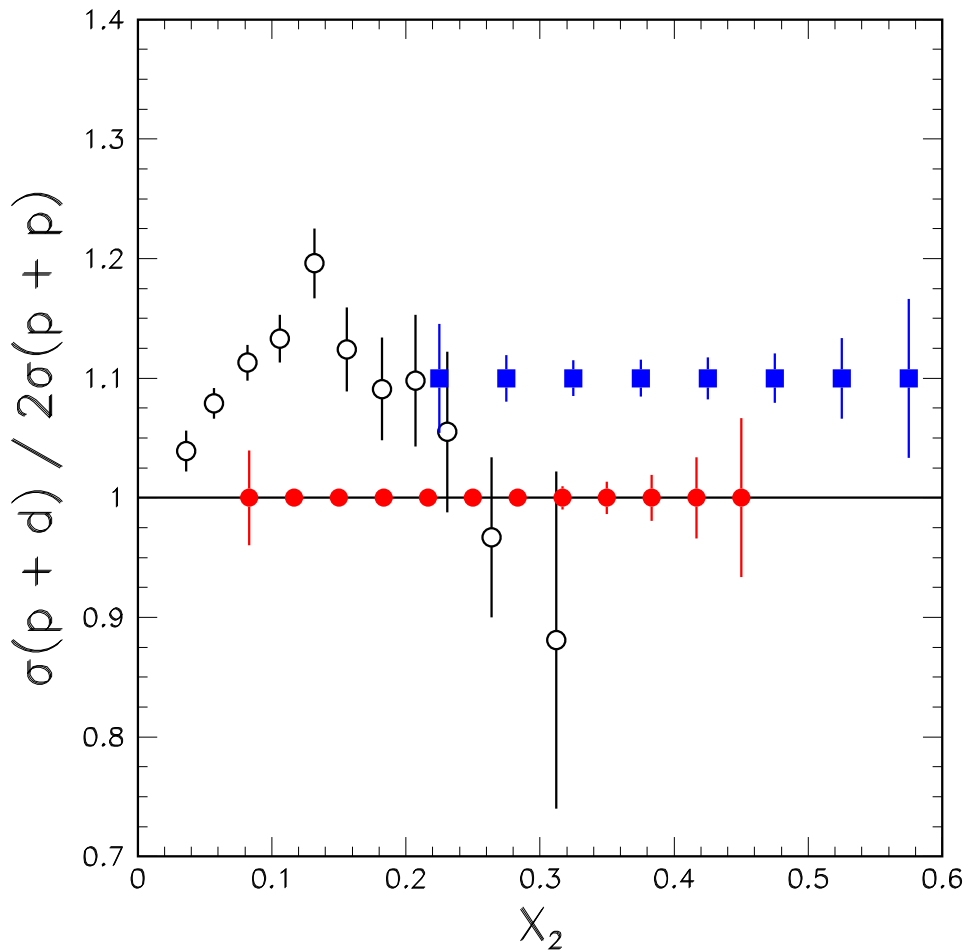


Figure 5:  $(p + d)/(p + p)$  Drell-Yan ratios from E866 (open circles) are compared with the expected sensitivities at the 120 GeV Main Injector (solid circles) and the 50-GeV PS (solid squares).

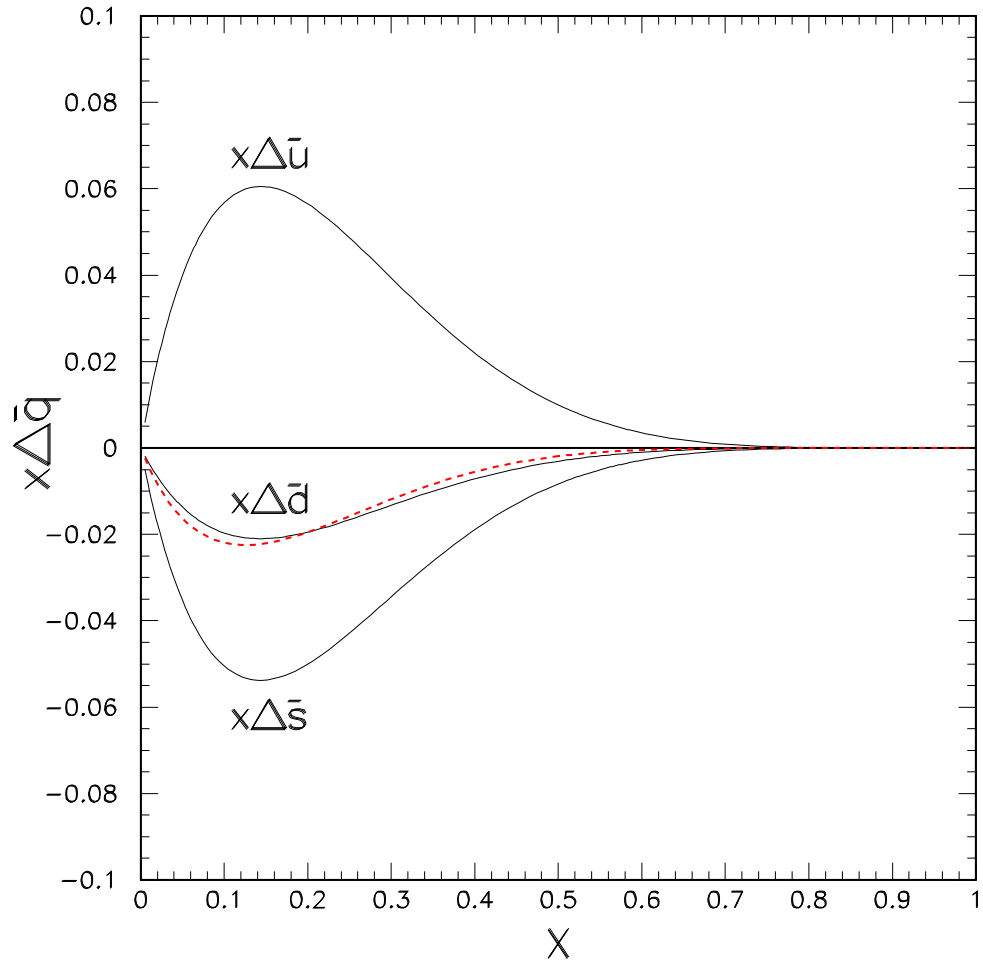


Figure 6: Sea quark polarizations at  $Q^2=0.36$  GeV $^2$  predicted by chiral-quark soliton model are shown as solid curves. The dashed curve corresponds to the parametrization of  $x\Delta\bar{q}$  at  $Q^2 = 0.4$  GeV $^2$  by GRSV, where  $\Delta\bar{q} = \Delta\bar{u} = \Delta\bar{d} = \Delta\bar{s}$ .

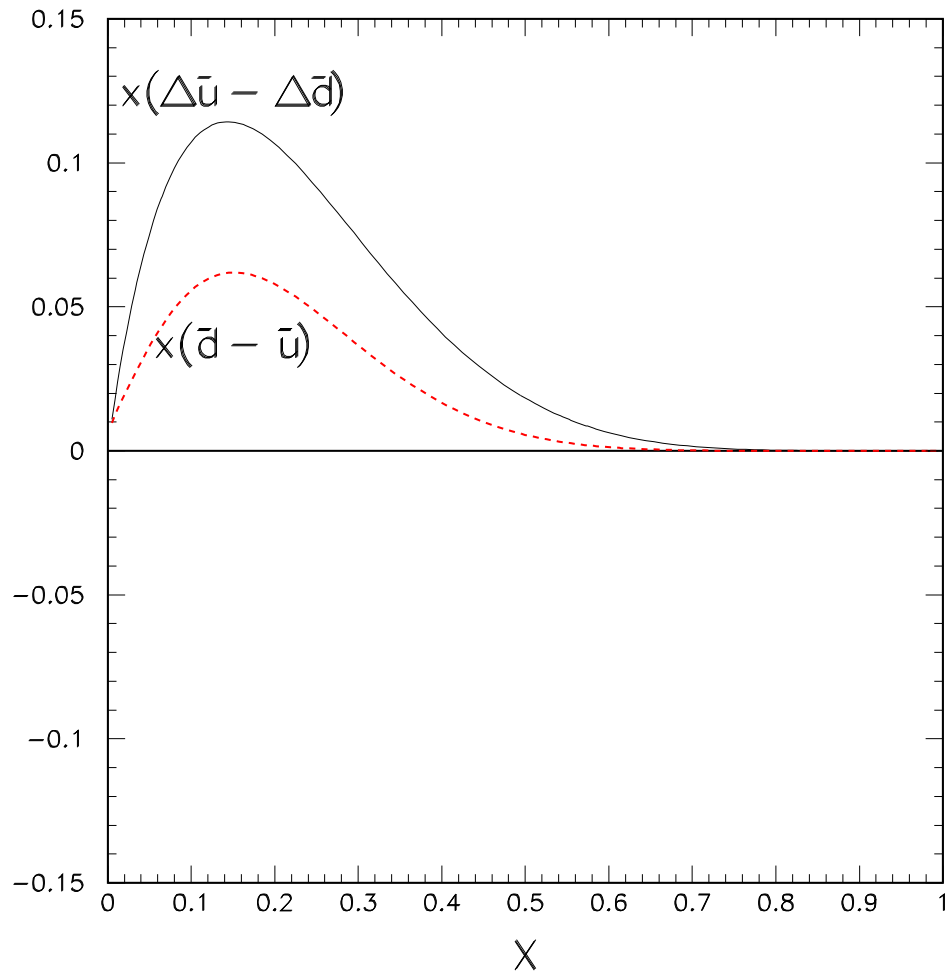


Figure 7:  $x(\Delta\bar{u} - \Delta\bar{d})$  at  $Q^2 = 0.36 \text{ GeV}^2$  predicted by the chiral-quark soliton model is shown as the solid curve. The GRV94 LO parametrization of  $x(\bar{d} - \bar{u})$  at  $Q^2 = 0.4 \text{ GeV}^2$  is shown as the dashed curve.

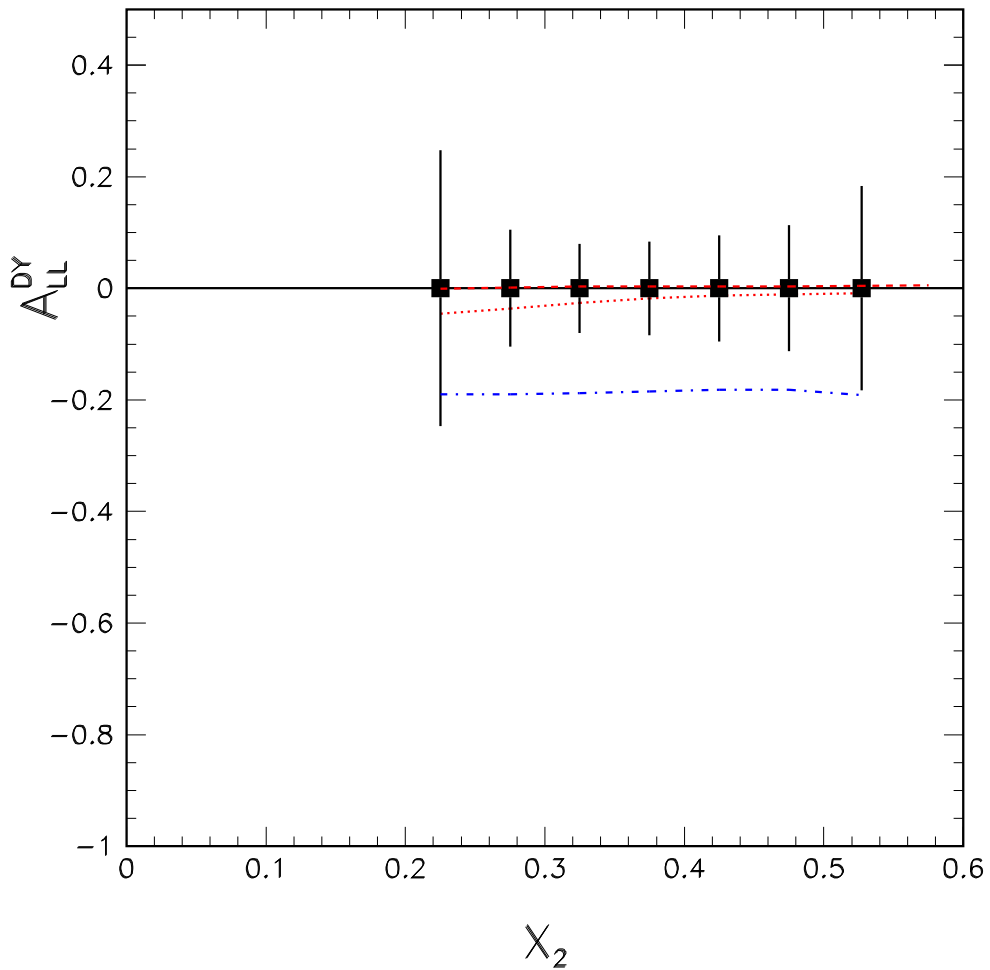


Figure 8: Expected statistical accuracy for measuring the double-helicity asymmetry  $A_{LL}^{DY}$  in polarized  $p + p$  Drell-Yan at the 50-GeV PS for a 120-day run. The dashed, dotted, and dash-dotted curves correspond to calculations using polarized PDF parametrization of G-S (set A, set C) and GRSV, respectively.

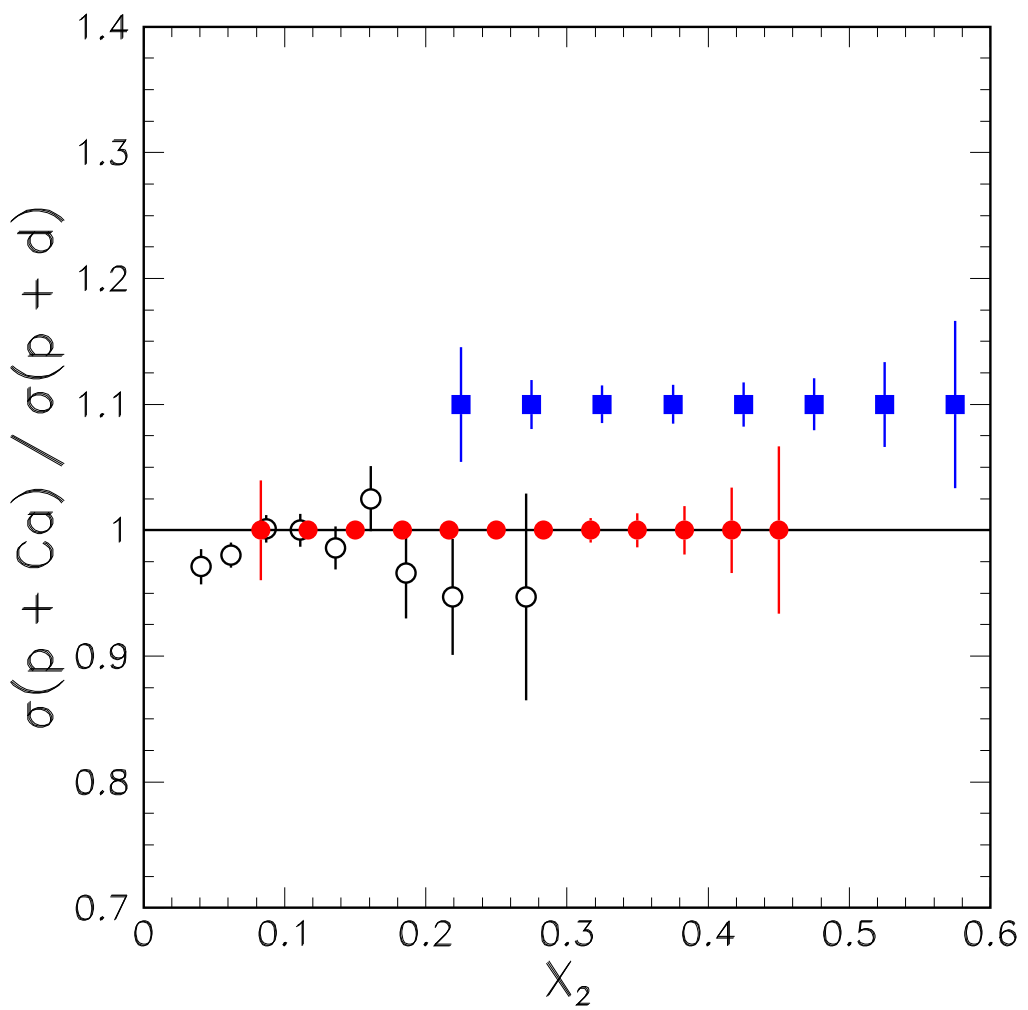


Figure 9:  $(p + Ca)/(p + d)$  Drell-Yan ratios from E772 (open circles) are compared with the expected sensitivities at the 120 GeV Main Injector (solid circles) and at the 50 GeV PS (solid squares).

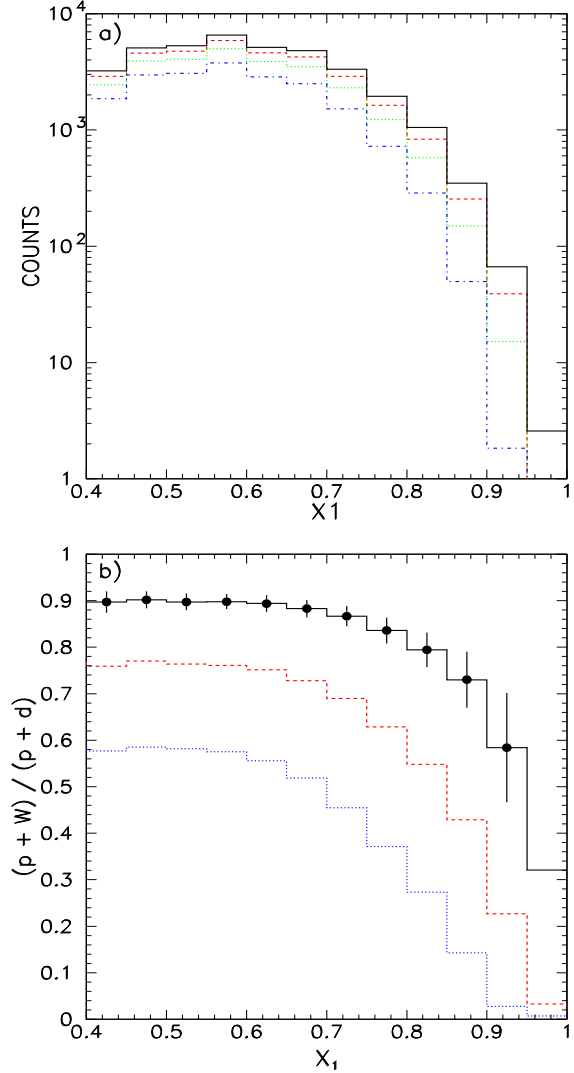


Figure 10: a): Solid curve is the expected  $p+d$  spectrum for a 60-day run at 50 GeV. The dashed, dotted, and dash-dotted curves correspond to  $p+W$  spectra assuming a partonic energy loss rate of 0.1, 0.25, 0.5 GeV/fm, respectively. b): Solid circles show the expected statistical errors for  $(p+W)/(p+d)$  ratios in a 60-day run for  $p+W$  and  $p+p$  each. The solid, dashed, and dotted curves correspond to a partonic energy loss rate of 0.1, 0.25, 0.5 GeV/fm, respectively.

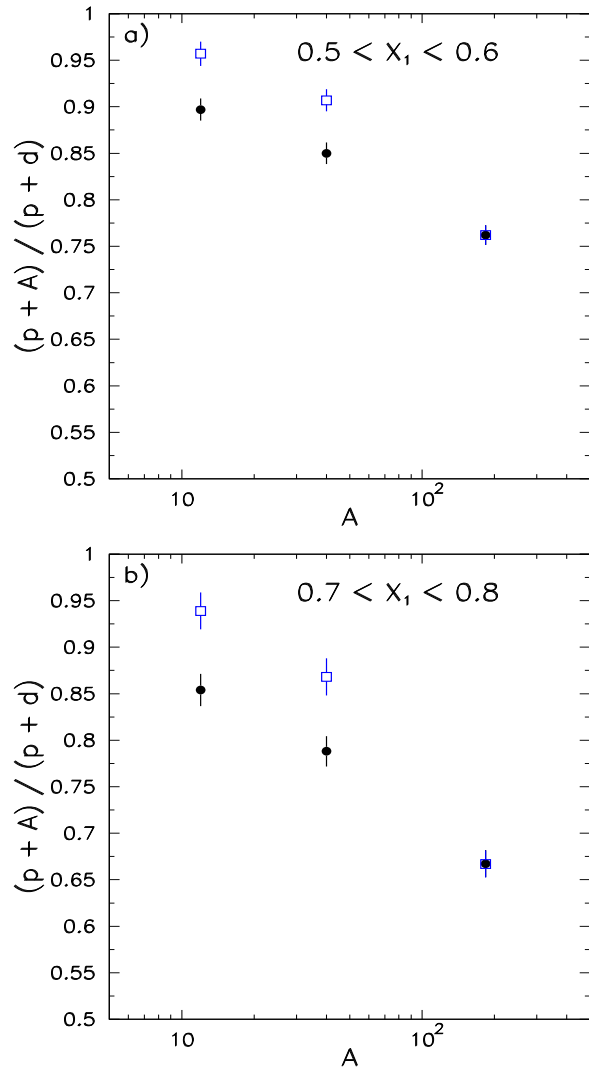


Figure 11: a): Solid circles correspond to the expected  $(p + A)/(p + d)$  ratios assuming a partonic energy loss rate of 0.25 GeV/fm with a nuclear dependence given by Eq. 10. The open squares correspond to partonic energy loss given by Eq. 11. The statistical errors were calculated assuming a 60-day run for each target. b) Same as the top figure, but for a different  $x_1$  bin ( $0.7 < x < 0.8$ ).

$P + D \rightarrow J/\Psi + X$  at 50 GeV

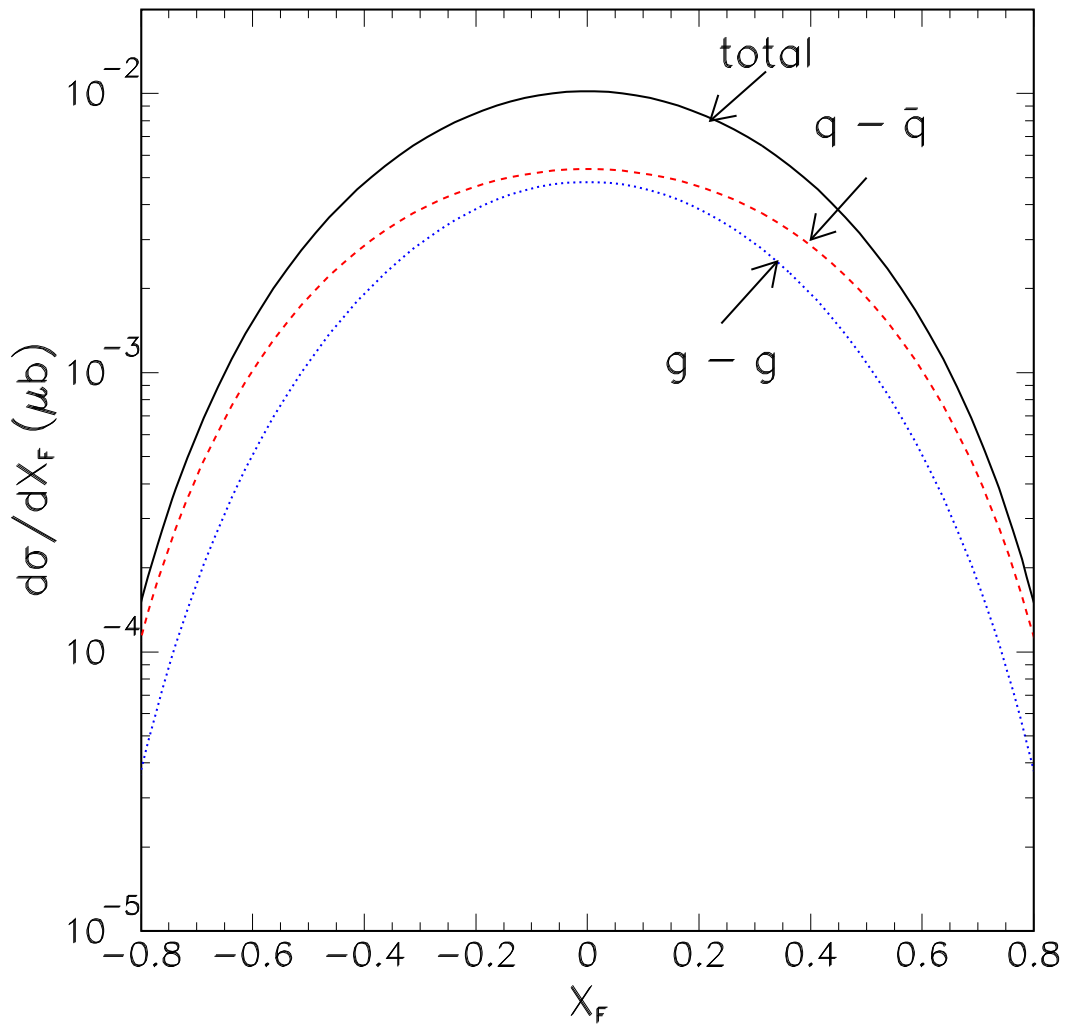


Figure 12: Calculation of the  $p + d \rightarrow J/\Psi + x$  cross sections at 50 GeV using the color-evaporation model. The contributions from the gluon-gluon fusion and the quark-antiquark annihilation subprocesses are also shown.

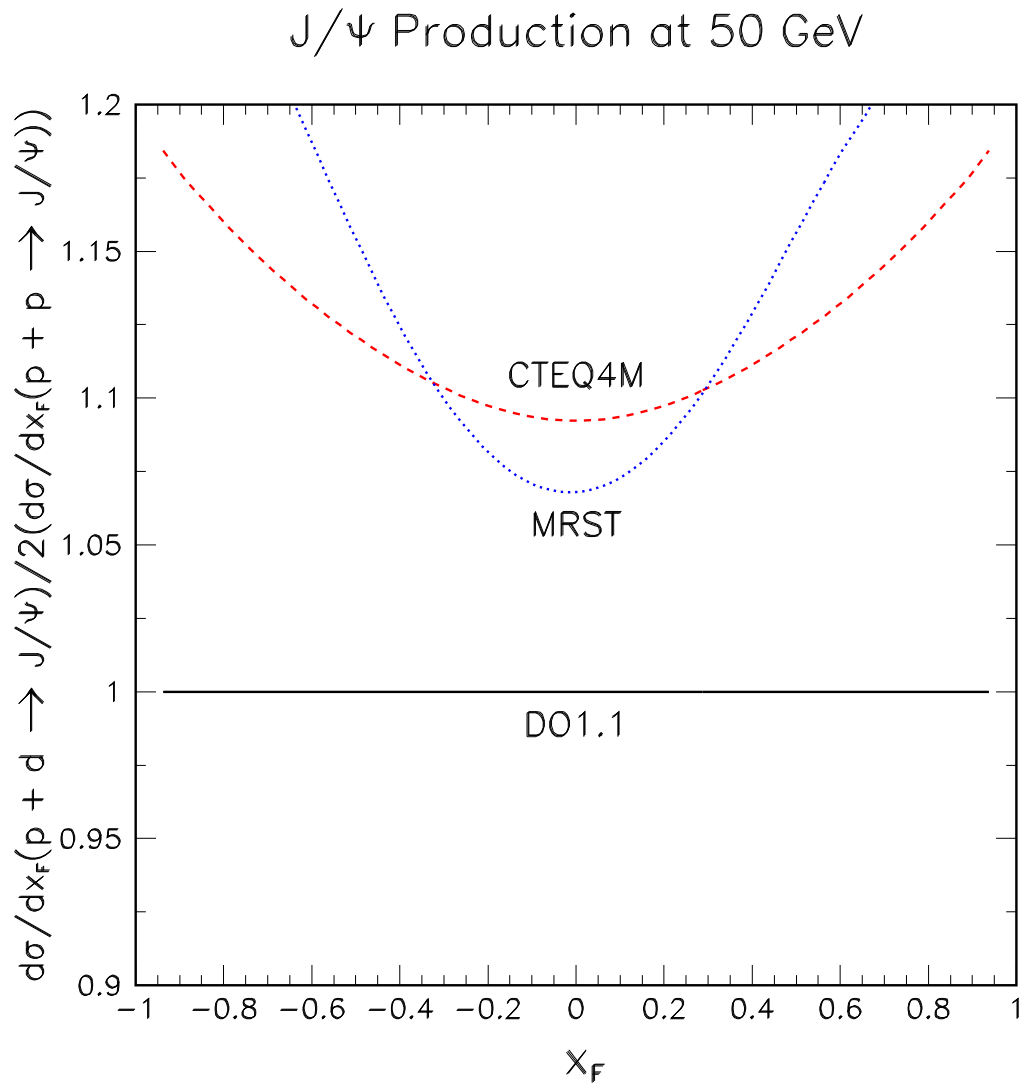


Figure 13: Calculations of the  $p + d \rightarrow J/\Psi$  over  $p + p \rightarrow J/\Psi$  ratios at 50 GeV using the color-evaporation model. The  $\bar{d}/\bar{u}$ -symmetric structure functions DO1.1 and the  $\bar{d}/\bar{u}$  asymmetric structure functions (MRST and CTEQ4M) have been used in these calculations.

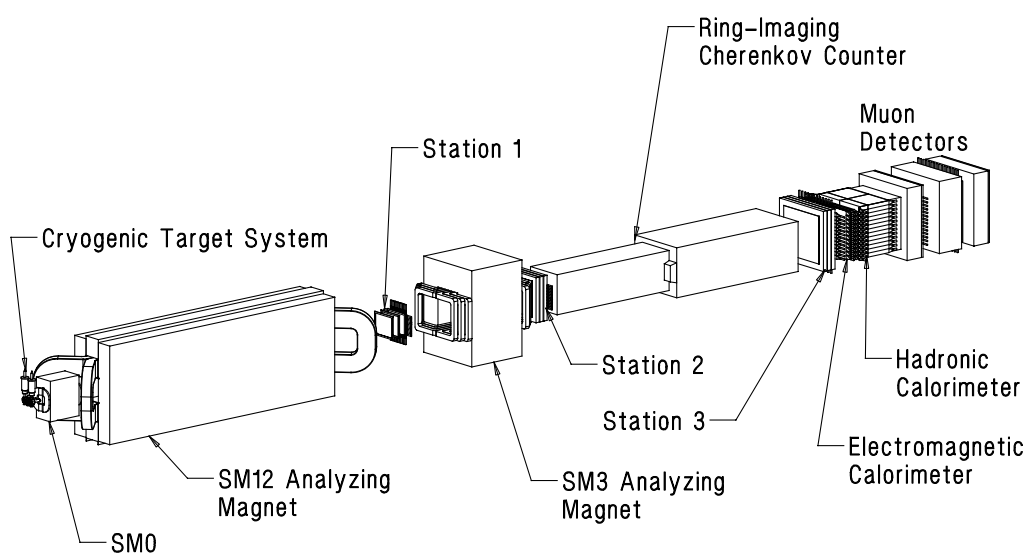
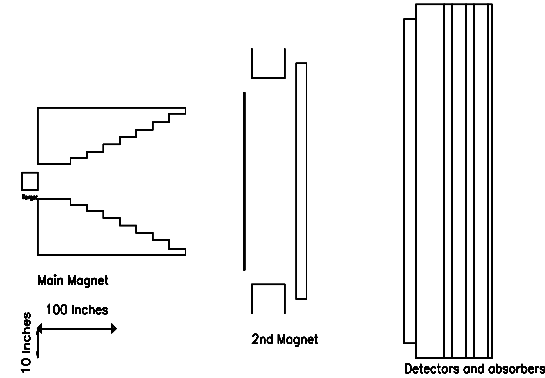


Figure 14: Schematic layout of the Meson-East focusing spectrometer at Fermilab.

Schematic view in horizontal plane



Schematic view in vertical plane

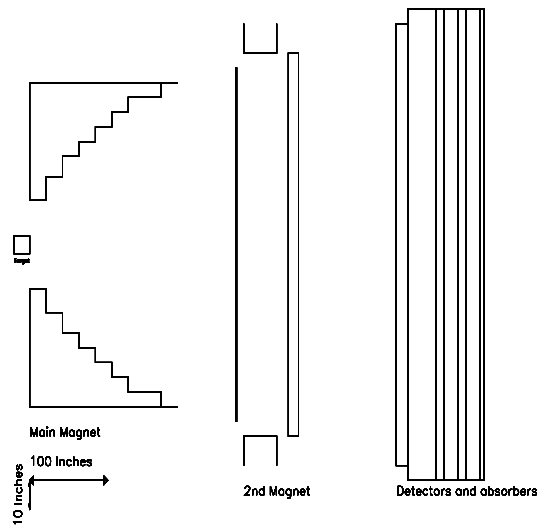


Figure 15: A schematic view of the prototype spectrometer. The top is the horizontal view and the bottom is the vertical view.